Passive Phase-Distortionless Parametric Limiting with Varactor Diodes*

I. T. HO† AND A. E. SIEGMAN†, MEMBER, IRE

Summary—**The theory of passive parametric limiting with a varactor diode as the nonlinear element is developed and verified experimentally. The limiting is found to be flat and phase-distortionless. Expressions are given for threshold level, dynamic range, bandwidth, and power dissipation. The transient phenomena, comprising leading- and trailing-edge leakage spikes, are studied theoretically and experimentally, and found to be small in typical instances. Experimental results reported upon include a simple waveguide limiter structure at *S* band; a lumped-circuit limiter at 126 Mc; and a strip-line limiter using a pill varactor at *S* band. The latter has an insertion loss of 2.5 db below threshold, a threshold level of 2 mw, a dynamic range in excess of 20 db, and less than 5° of phase distortion. Agreement between theory and experimental results is excellent.**

Introduction

A METHOD of obtaining flat and phase-distortionless limiting in a passive parametric circuit was proposed some time ago by one of the authors [1]. Several experimental verifications of this idea, using varactor diodes as the parametric element, have since been reported [2], [3], [6]. In the present paper, we present a more detailed analysis of the diode type of passive parametric limiter, including both steady-state and transient behavior. We also present experimental results from several such limiters which closely confirm the theoretical predictions.

To describe the operation of this type of limiter, one may suppose that there is coupling between a signal frequency (ω) tank and a subharmonic frequency ($\omega/2$) tank through a nonlinear coupling element, as shown in Fig. 1. When the input signal power at ω is smaller than a certain threshold level P_{th}, the ω tank may be treated as an ordinary resonant circuit inserted between the input and the output. However, above this threshold level, which is the level just sufficient to excite the system into oscillation at the subharmonic frequency, a sharp limiting action occurs in the ω tank. Any further increase in the input signal above the threshold level does not appear in the output, but is partially transferred into the subharmonic oscillations and partially reflected back to the power source due to an increased impedance mismatch between the source and the ω tank. The general behavior is shown in Fig. 2.

The ideal output is limited abruptly and flatly beyond the threshold level until the input power increases

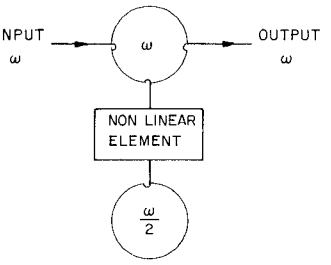

Fig. 1—Schematic of a passive parametric limiter.

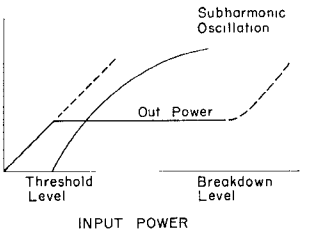

Fig. 2—General characteristics of a passive parametric limiter.

to some breakdown level P_{br}. The breakdown level for the varactor diode limiter occurs when the sum of the dc bias and the RF voltage is either larger than the reverse breakdown voltage of the varactor diode, or else is large enough to drive the varactor diode into its forward conduction region. In either case, this creates a more complicated situation, and the limiting action then generally deteriorates.

When a square-wave-modulated input signal whose amplitude is larger than the threshold level is applied to a parametric limiter, the output will be of fixed amplitude and phase-distortionless in the steady-state region, at least in the ideal case. However, the output signal will also show transient phenomena, including both a leading-edge leakage spike and a trailing-edge leakage spike. The leading-edge spike is formed because the subharmonic oscillations take time to build up from thermal noise, and the limiting action does not occur until the subharmonic oscillations have built up to a substantial value. The trailing-edge leakage spike is formed because energy stored in the subharmonic oscillation reconverts itself into the signal frequency when the input signal is turned off. In general, the leading-edge spike is found to represent more energy than the trailing-edge one.

In the ideal square-wave input case, the height of the leading-edge leakage spike is equal to the non-limited amplitude of the input signal, while the duration of the spike decreases as the input signal amplitude is in-

* Received by the PGMTT, May 1, 1961. The work reported in this paper was supported by the Wright Air Development Div. of the U. S. Air Force under Contract AF33(616)-6207, and is taken in large part from a Ph.D. dissertation submitted to the Dept. of Elec. Engrg., Stanford University, Stanford, Calif., by I. T. Ho.

† Stanford Electronics Laboratory, Stanford University, Stanford, Calif.

creased. Thus, as the input level is increased, the leakage spike gets higher but shorter, according to both theory and experiment. However, it is also found that when a realistic square-wave-modulated input signal with a finite rise time is applied to the limiter, the amplitude of the leading-edge spike does not increase indefinitely as input power increases, but rather approaches a saturation level.

In this paper: 1) the governing equations for the varactor diode parametric limiter are derived and solved in the steady-state case and design data for such limiters developed; 2) solutions of the governing equations in the transient case are summarized in order to show the nature and governing parameters of the initial and final leakage spikes; 3) this transient analysis is carried further in order to study the transient response to a finite rise time input, and to show the resulting saturation of the initial leakage spike; 4) experimental data are given for diode limiters operating in the VHF and microwave bands. Besides illustrating the possibilities of the parametric limiter as a useful device, these results also verify the theoretical analysis in detail.

It should be noted that essentially this same parametric limiting mechanism is responsible for the limiting action observed in ferrites and garnet-sphere devices at high power levels [4], [5], [14]. In these cases, various spin-wave modes play the role of the half-frequency tank. The analysis given here is thus also relevant to the ferrite case to some extent, with appropriate modifications. However, the ferrite case is generally somewhat more complicated because the spin waves furnish not one but many subharmonic resonant modes.

Comparison should be made between this work and the varactor diode parametric limiting results recently published by Olson and Wade [7], [16]. The two cases are, of course, quite different, the present limiter being an entirely passive "self-pumped" device, while Olson and Wade consider the signal-limiting properties of the standard parametric amplifier or frequency converter with the usual separate pumping signal. The best experimental results obtained by Olson and Wade considerably surpass the results obtained in this work at least in dynamic range, their limiter yielding a dynamic range of limiting in excess of 50 db in a two-stage limiter, as compared with ~20 db in our best one-stage limiter. In addition, their device has 10 db of gain below the limiting level as compared to $2\frac{1}{2}$ db of loss below threshold in our passive limiter, and the passive limiting threshold is considerably higher (although still in the milliwatt range). The passive device has a number of significant advantages, however. It is, of course, passive, requiring no pumping source, and also having none of the pump instability problems of other parametric devices. Its construction is much simpler with many fewer elements involved, and the setup and tuning is very simple, in contrast to the rather careful tuning and adjustment procedures which led to Olson and Wade's optimum results. The bandwidth of the passive limiter appears to be much wider. Finally, the dynamic range of the passive limiter can also be made substantially larger than the results reported here, both by using two such limiters in cascade and also by using a varactor diode with a larger reverse breakdown voltage.

Circuit Model and Governing Equations

When a reverse bias V_0 plus an RF voltage v is applied to a nonlinear capacitance diode, the instantaneous diode capacitance can be written in Taylor series form as $C(V)=C(V_0)+Dv+D_2v^2+$higher-order terms. The negative bias is typically $V_0=-2$ to -3 volts, and the RF voltage v is not larger than this if the diode is not driven into its forward conduction or reverse breakdown regions. Under these conditions, it can be shown that for typical $C(V)$ curves [9], the D_2v^2 term in the expansion is small compared to the Dv term, and we can drop the second and all higher-order terms.

From Fig. 1, the circuit model for a parametric limiter should consist of two resonant tanks plus a varactor diode. Fig. 3 shows the equivalent circuit used in this work. In this circuit,

L_1 and $L_{1/2}$ denote the inductances of the ω and $\omega/2$ tanks;

C_1 and $C_{1/2}$ denote the total capacitances in the ω and $\omega/2$ tanks, including the dc portion of the varactor diode capacitance in each case;

$G_{1/2}$ denotes the total internal loss conductance of the $\omega/2$ tank including losses due to the diode;

G_1 denotes the internal loss conductance of the ω tank including the diode losses, G_g and G_L denote the source and load conductances connected to this tank, and $G_T=G_1+G_g+G_L$ denotes the total conductance in the ω tank;

and $C=Dv$ denotes the nonlinear portion of the varactor diode capacitance.

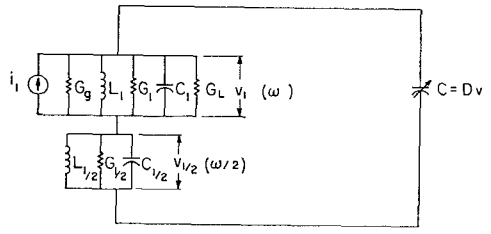

Fig. 3—Circuit model for a varactor diode parametric limiter.

We have followed the conventional practice in parametric analysis [7], [10] of including the dc portions of the diode admittance in the resonant tanks. The current source i_1 is the input signal source.

Assume that both the ω and $\omega/2$ tanks have Q's much larger than unity. Then at the ω frequency, the $\omega/2$ tank will look like a short circuit while at $\omega/2$, the ω tank will also look like a short circuit. With this assumption, we write the usual integro-differential equations for the circuit, taking one additional differentiation to get rid of integral signs. The governing circuit equations for the ω and the $\omega/2$ frequencies are then

$$C_1d^2v_1/dt^2+G_Tdv_1/dt+\Gamma_1v_1=di_1/dt-d^2(Cv)/dt^2$$
$$C_{1/2}d^2v_{1/2}/dt^2+G_{1/2}dv_{1/2}/dt+\Gamma_{1/2}v_{1/2}=-d^2(Cv)/dt^2, \quad (1)$$

where $v=v_1+v_{1/2}$ is the total RF voltage at ω and $\omega/2$, $\Gamma=L^{-1}$, and only the appropriate frequency components from the $d^2(Cv)/dt^2$ term are to be included in each equation. The voltages at ω and $\omega/2$ are now written in terms of their assumed slowly varying phasor amplitudes as $v_1(t)=V_1(t)\exp(j\omega t)+V_1^*(t)\exp(-j\omega t)$ and $v_{1/2}(t)=V_{1/2}(t)\exp(j\omega t/2)+V_{1/2}^*(t)\exp(-j\omega t/2)$, and the driving current is written as $i_1(t)=I_1(t)\exp(j\omega t)+I_1^*(t)\exp(-j\omega t)$. Inserting these into (1) and neglecting certain terms on the assumption that $dV/dt \ll \omega V$ leads to the following equations for the slowly varying amplitude terms:

$$\frac{dV_1}{dt}+\frac{\omega}{2Q_T}V_1+j\frac{\omega D}{2C_1}V_{1/2}^2=\frac{I_1}{2C_1}+j\frac{1}{2\omega C_1}\frac{dI_1}{dt} \tag{2}$$

and

$$\frac{dV_{1/2}}{dt}+\frac{\omega}{4Q_{1/2}}V_{1/2}+j\frac{\omega D}{2C_{1/2}}V_{1/2}^*V_1=0, \tag{3}$$

where $Q_T=\omega C_1/G_T$ is the loaded Q of the ω tank, and $Q_{1/2}=\omega C_{1/2}/2G_{1/2}$ is the Q of the $\omega/2$ tank. These equations are for the case where ω is exactly on resonance. Additional reactive terms are present in both equations when ω is off resonance. Eqs. (2) and (3) are the basic equations for the analysis of the parametric limiter.

For simplicity, we have treated here only the degenerate case in which the subharmonic oscillation is at exactly half the signal frequency. The limiting mechanism is also operable with the subharmonic oscillation occurring simultaneously at two different lower frequencies which add up to the signal frequency, and such operation has been observed [6]. Limiter design and construction, as well as analysis, would seem to be simplest in the degenerate case, however.

Steady-State Solutions and Design Formulas

Limiting Action and Threshold Level

The steady-state behavior of the limiter is obtained by setting the time derivatives in (2) and (3) to zero. Assuming for the moment an applied signal exactly on resonance, these equations can be manipulated to yield

$$V_1=j\frac{G_{1/2}}{\omega D}\frac{V_{1/2}}{V_{1/2}^*} \tag{4}$$

and

$$V_{1/2}^2=\frac{-j}{\omega D}(I_1-G_TV_1). \tag{5}$$

Below threshold, there are no subharmonic oscillations, $V_{1/2}$ is zero, and hence (4) is indeterminate. Eq. (5), however, gives $I_1=G_TV_1$, *i.e.*, the ω tank is unaffected by the $\omega/2$ tank, and V_1 and I_1 are in phase. Above threshold it is immediately apparent from (4) that V_1 has a constant value independent of the magnitude of $V_{1/2}$ or, in other words, V_1 limits. Since, in the shunt model used, V_1 is the voltage across the load conductance G_L, the power output from the device also limits.

More precisely, above threshold we can write $V_{1/2}=|V_{1/2}|\exp(j\theta_{1/2})$. It is convenient to choose the origin of time such that $\theta_{1/2}$ has either of the values $-\pi/4$ or $+3\pi/4$. Substituting this into (4) then makes V_1 a real and positive quantity given by

$$V_1=V_{th}=\frac{G_{1/2}}{\omega D}=\frac{V_d}{2Q_{1/2}}, \tag{6}$$

where it is convenient to introduce the parameter $V_d\equiv C_{1/2}/D$ which indicates the relative amount of nonlinearity in the $\omega/2$ tank. When the varactor diode is strongly coupled to the microwave circuitry employed in the limiter (*i.e.*, the "filling factor" is large, which is the optimum situation), $C_{1/2}$ will consist primarily of the dc capacitance of the varactor diode itself, and V_d will have a minimum value characteristic of the diode only. This, then, serves as a figure of merit for the varactor diode in parametric limiter applications. As an example, for a Microwave Associates MA4253 diode operated at -1 volt bias in a strip-line circuit, this quantity is $V_d\sim 40$ volts.

The two possible choices of phase for the subharmonic oscillations illustrate the well-known bistable phase condition for parametric subharmonic oscillations, as employed for example in the parametron computer element [12], [13]. With either choice, (5) can be rewritten as

$$|V_{1/2}|^2=\frac{1}{\omega D}(I_1-G_TV_{th}), \tag{7}$$

which shows how the subharmonic oscillations increase in amplitude as I_1 is raised above the threshold value I_{th} given by

$$I_{th}=G_TV_{th}=\frac{G_TV_d}{2Q_{1/2}}. \tag{8}$$

Note that both $|V_{1/2}|^2$ and V_{th} in (7) are purely real quantities, and therefore, I_1 must also be a purely real quantity. This indicates that I_1 and V_1 have the same phase above and below threshold, or in other words the limiting action is phase-distortionless, at least for signals applied exactly on resonance.

Finally, the input power level corresponding to the limiting threshold is given by

$$P_{th}=\frac{I_{th}^2}{2G_g}. \tag{9}$$

This quantity is given in a more useful form in the following section.

Insertion Gain, Input VSWR, and Power Distribution

The power insertion gain $L_0(\leq 1)$ of the limiter below threshold is given by the standard expression for a transmission cavity, namely

$$L_0=\frac{4Q_T^2}{Q_{eg}Q_{eL}}=\frac{4G_gG_L}{(G_g+G_1+G_L)^2} \tag{10}$$

where Q_{eg} and Q_{eL} are the external Q's of the input and output couplings from the ω tank, respectively. The threshold power level can be rewritten from (9) and (8) as

$$P_{th} = \frac{V_d^2}{8Q_{1/2}^2}\left[\frac{(G_g + G_1 + G_L)^2}{G_g}\right]. \tag{11}$$

If the source conductance is taken to be variable (*i.e.*, by varying the degree of coupling between the signal source and the ω tank), the insertion gain is found to be maximized and the threshold power level minimized by the same condition, namely that the source be matched to the limiter, or $G_g = G_1 + G_L$. If this condition is satisfied, the insertion loss becomes

$$L_0 = \frac{G_L}{G_1 + G_L} = \frac{Q_1}{Q_1 + Q_{eL}}. \tag{12}$$

This can be made close to unity by making $Q_{eL} \ll Q_1$, *i.e.*, by making the external loading heavy compared to the unloaded Q. The optimizing condition requires that the input coupling also be made heavy. With optimum input coupling, the threshold power can be thrown into the form

$$P_{th} = \frac{1}{1 - L_0}\frac{V_d^2 G_1}{2Q_{1/2}^2} = \frac{1}{1 - L_0} P_{th(\min)}. \tag{13}$$

There is a minimum threshold power given by $P_{th(\min)} = V_d^2 G_1 / 2Q_{1/2}^2$. If the diode is tightly coupled to the limiter circuitry, G_1 will consist primarily of the equivalent shunt conductance of the varactor diode itself, and $Q_{1/2}$ will be essentially equivalent to the Q of the varactor diode. Therefore, this minimum threshold power is essentially a property of the varactor diode only. As a typical example, the numbers involved might be $V_d = 40$ volts, $G_1 = 4 \times 10^{-3}$ mhos, and $Q_{1/2} = 100$, leading to a threshold power of 0.3 mw. Varactor diode limiters can thus have respectably low limiting levels.

Eq. (13) shows, however, that the actual threshold power is greater than this minimum value by an amount depending on how close the insertion gain is made to unity. Fig. 4 plots the ratio $P_{th}/P_{th(\min)}$ in db as a function of the insertion gain in db. The quantity Q_1/Q_{eL} (or $Q_1/Q_{eg} = Q_1/Q_{eL} + 1$) is, of course, the parameter which moves one along this curve.

Above the threshold level, the effect of the $\omega/2$ tank and the subharmonic oscillations on the ω tank may be accounted for by introducing into the ω tank an additional effective conductance G_{add} which increases with input power in such a way as to keep V_1 constant at V_{th} when I_1 increases above I_{th}. This additional conductance is given by

$$\begin{aligned} G_{\text{add}} &= \frac{I_1}{V_1} - G_T \\ &= (I_1/I_{th} - 1)G_T \\ &= (n - 1)G_T, \end{aligned} \tag{14}$$

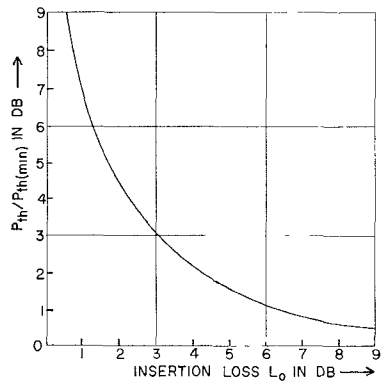

Fig. 4—Increase in threshold power above the minimum value, as a function of the below-threshold insertion loss L_0.

where $n = I_1/I_{th}$ is a measure of how far the input power is increased above threshold. As a result of this additional conductance, the input impedance of the limiter as seen by the signal source changes. The signal source in most practical cases will probably be undercoupled to the limiter, since the Q of the limiter is generally limited by the diode Q and is not large. With this assumption, the magnitude of the reflection coefficient looking from the signal source towards the limiter above threshold can be written

$$\rho = \frac{G_1 + G_L + G_{\text{add}} - G_g}{G_1 + G_L + G_{\text{add}} + G_g} = \frac{\rho_0}{n} + \frac{n - 1}{n}, \tag{15}$$

when ρ_0 is the reflection coefficient below the threshold level. The input voltage-standing-wave ratios above and below threshold, S and S_0, are thus related by

$$S = nS_0 + (n - 1). \tag{16}$$

Experimental verification of this equation will be given below.

The input power to the limiter above threshold is distributed among the following four outlets: 1) output power; 2) power losses in the ω tank; 3) power losses in the $\omega/2$ tank due to the subharmonic oscillations; and 4) power reflected from the limiter back to the signal source or to an isolator placed in the input line. Power losses 2) and 3) are dissipated chiefly by the diode in practical cases, since the diode losses generally predominate over copper losses if the diode is tightly coupled. If we assume for simplicity that the limiter input below threshold is matched, as required for optimum performance, then the powers into each of these four categories are given by the simple expressions

$$\begin{aligned} P_{\text{out}} &= 2V_{th}^2 G_L = L_0 P_{th}, \\ P_{\text{loss}}(\omega) &= 2V_{th}^2 G_1 = (1 - L_0)P_{th}, \\ P_{\text{loss}}(\omega/2) &= 2V_{th}^2 G_{\text{add}} = 2(n - 1)P_{th}, \\ P_{\text{reflected}} &= \rho^2 P_{\text{in}} = (n - 1)^2 P_{th}. \end{aligned} \tag{17}$$

These four powers are plotted in Fig. 5 as a function of the input power below and above threshold. It is appar-

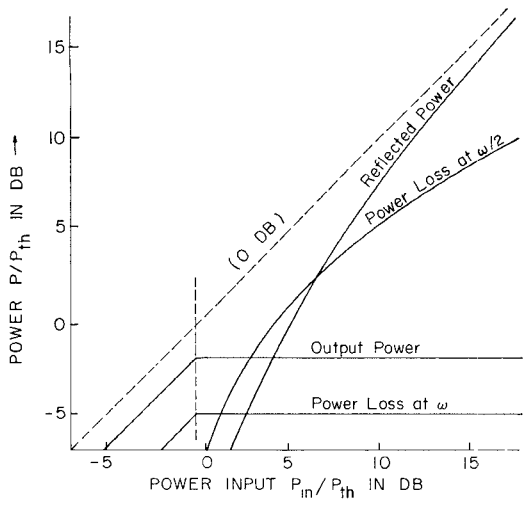

Fig. 5—Distribution of input power among various outlets, as a function of the input power level, assuming an insertion loss of 2.5 db below threshold.

ent that above the threshold, the largest amount of power is reflected, although the diode must also absorb some power at higher input power levels. This information is important in determining the maximum power input the limiter can withstand without damage to the varactor diode due to overload.

Dynamic Range

In the varactor diode limiter, the diode should not be driven either beyond its reverse breakdown voltage or into its forward conduction region, so that the sum of the dc bias and RF voltages must not go positive nor exceed the reverse breakdown voltage $-V_{br}$. The desirable reverse bias for the diode is thus $V_0 \approx -V_{br}/2$, and the total instantaneous RF voltage must then not exceed $V_{br}/2$. Although the total RF voltage is the sum of v_1 and $v_{1/2}$, it can be shown that $v_{1/2}$ is much the larger of the two when strong limiting action is occurring. Since the peak value of $v_{1/2}$ is $2|V_{1/2}|$, the condition for breakdown is

$$2|V_{1/2}| = \left[\frac{(n-1)2V_dV_d'}{Q_TQ_{1/2}}\right]^{1/2} \leq \frac{V_{br}}{2}, \tag{18}$$

where $V_d' \equiv C_1/D$ is a parameter of the same nature as $V_d \equiv C_{1/2}/D$. In fact, if the diode is very tightly coupled to the limiter circuitry, the situation will be $C_1 \approx C_{1/2} \approx$ the dc capacitance of the varactor diode. Eq. (18) can be reversed to give the maximum allowable value of n as

$$n_{\max} = \frac{Q_TQ_{1/2}V_{br}^2}{8V_dV_d'} + 1. \tag{19}$$

The dynamic range of the limiter from threshold to breakdown is, then,

$$\text{Dynamic range} = 20 \log_{10} n_{\max}. \tag{20}$$

Over this range, the limiting in a good limiter should be essentially flat and phase-distortionless. One can, of course, drive the limiter even beyond this range, and limiting action will still be present. The limiting will not be ideal, however, and care must be taken that the diode is not damaged by excessive current or power dissipation.

Bandwidth

Assume now that the signal frequency ω is not exactly equal to the resonant frequency ω_0 of the signal tank. We then define

$$\Delta\omega = \omega - \omega_0 \qquad \Delta(\omega/2) = (\omega/2) - (\omega_0/2)$$
$$\delta = \Delta\omega/\omega_0 \qquad \delta_{1/2} = \Delta(\omega/2)/(\omega_0/2) = \delta. \tag{21}$$

We will assume here that the subharmonic tank is tuned to exactly one-half the signal tank, and that, as mentioned before, the subharmonic oscillation occurs in degenerate fashion at $\omega/2$ rather than at any two other frequencies adding up to ω.

Eq. (4) must now be modified to

$$V_1(\omega) = j\frac{Y_{1/2}}{\omega D}\frac{V_{1/2}}{V_{1/2}^*}, \tag{22}$$

where

$$Y_{1/2} = G_{1/2} + j(\omega C_{1/2}/2 - 2/\omega L_{1/2})$$
$$\approx G_{1/2}[1 + j2Q_{1/2}\delta]. \tag{23}$$

Eq. (22) indicates that V_1 is still ideally limited even when the signal is off resonance. If we make the same assumption as previously about the phase of $V_{1/2}$, the threshold voltage as a function of frequency will be given by

$$V_{th}(\omega) = V_{th}(\omega_0)[1 + j2Q_{1/2}\delta], \tag{24}$$

and the limited output power level will be

$$P_{\text{out}}(\omega) = P_{\text{out}}(\omega_0)\cdot[1 + 4Q_{1/2}^2\delta^2]. \tag{25}$$

The output power from the limiter operating above threshold has the form of an inverted resonance curve with Q value equal to the $Q_{1/2}$ of the subharmonic resonant circuit. Below threshold, of course, the limiter is simply a transmission cavity with power transmission given by the usual expression

$$L(\omega) = L_0\frac{1}{1 + 4Q_T^2\delta^2}. \tag{26}$$

Combining (25) and (26) leads to a set of curves of power output vs frequency at various input power levels of the form shown in Fig. 6 where the particular choice of parameters used is $Q_{1/2} = Q_T$.

For signals off resonance, the equivalent of (5) is

$$V_{1/2}^2 = \frac{-j}{\omega D}(I_1 - Y_1V_1), \tag{27}$$

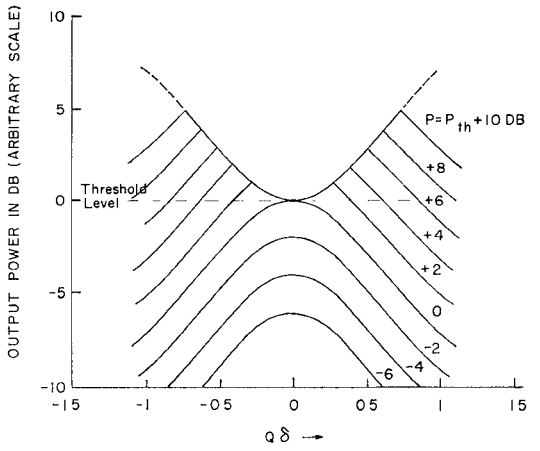

Fig. 6—Output power vs frequency for increasing power inputs (assuming $Q_T = Q_{1/2} = Q$).

where Y_1 is the admittance of the ω tank, approximately given by

$$Y_1 \approx G_T(1 + j2Q_T\delta). \tag{28}$$

The threshold value of I_1 off resonance is thus

$$\begin{aligned} I_{th}(\omega) &= Y_1(\omega)V_{th}(\omega) \\ &= I_{th}(\omega_0)[(1 + j2Q_T\delta)(I + j2Q_{1/2}\delta)], \end{aligned} \tag{29}$$

and the threshold input power off resonance is

$$P_{th}(\omega) = P_{th}(\omega_0)\cdot[(1 + 4Q_T{}^2\delta^2)(1 + 4Q_{1/2}{}^2\delta^2)]^{1/2}. \tag{30}$$

The threshold input power increases both because a larger voltage V_1 is required off resonance, and also because a larger power input is required to create this voltage off resonance.

Using the same choice as before for the origin of time or the phase of $V_{1/2}$ permits (27) to be put in the form

$$I_1(\omega) = Y_1(\omega)V_{th}(\omega) + \omega D\,|\,V_{1/2}\,|^2. \tag{31}$$

Below and at threshold the phase relationship between I_1 and V_1 is that appropriate to $Y_1(\omega)$. Above threshold, the phase relationship is determined by the preceding equation. It is apparent that as I_1 and $|\,V_{1/2}\,|$ increase above the threshold level, this phase relationship will be altered. Therefore, the limiting is no longer perfectly phase-distortionless off resonance; the amount of phase distortion increases with input level and with distance from resonance.

Second Order Effects

If the next higher order term D_2v^2 in the nonlinear capacitance expression is retained in the theory, it can be shown that the resulting steady-state equations analogous to (4) and (5) are

$$\begin{aligned} &\frac{\omega}{4Q_{1/2}}V_{1/2} + j\frac{\omega D}{2C_{1/2}}V_{1/2}{}^*V_1 \\ &\qquad = \frac{3D_2\omega^2}{4}[2\,|\,V_1\,|^2 + |\,V_{1/2}\,|^2]V_{1/2} \end{aligned} \tag{32}$$

$$\begin{aligned} &\frac{\omega}{2Q_T}V_1 + j\frac{\omega D}{2C_1}V_{1/2}{}^2 \\ &\qquad = \frac{I_1}{2C_1} + 3D_2\omega^2[2\,|\,V_{1/2}\,|^2 + |\,V_1\,|^2]V_1. \end{aligned} \tag{33}$$

It can then be shown from these equations that the limiting is no longer ideally flat, the power out vs power in characteristic showing a slight upward tilt.

Transient Solutions and Leakage Spikes

The ferrite type of parametric limiter exhibits relatively large and troublesome leakage spikes [4], [5], [14]. Such leakage spikes are not generally found to be nearly as troublesome in the varactor diode type of limiter. Nonetheless, detailed studies of the transient solutions to the governing equations (2) and (3) were carried out as part of this investigation, solutions being obtained both by numerical calculation and by deriving iterated piecewise analytical solutions. A very brief summary of these results is presented here. The detailed results can be found in the original report [2].

Nature of the Spikes

When an input signal pulse with a very steep leading edge is applied to the parametric limiter, the output at ω will at first build up very rapidly to the appropriate nonlimited level, the rate of buildup being determined only by the usual energy buildup considerations for a resonant circuit. If the input signal is far above threshold, the output will, of course, far exceed the steady-state limiting level of the device. The subharmonic oscillations at the same time begin to build up from their thermal noise level towards their steady-state value. The subharmonic buildup is essentially exponential with time, except for a very brief initial period when the energy in the ω tank is still being established. The rate of rise of the $\omega/2$ oscillations is determined by the strength of the "pumping" done by the input signal, the rate of rise being faster the farther the input signal is above the limiting threshold. As soon as the subharmonic oscillations reach nearly to their steady-state value, the limiting action begins, and the signal level in the ω tank very rapidly drops to the steady-state limited value. The signal output thus exhibits an initial leakage spike whose height increases directly with input signal level and whose duration decreases with increasing input level.

If the input signal is suddenly turned off after the limiter has reached the steady-state condition, the device is left with a substantial amount of energy stored in the subharmonic resonant circuit. Some of this energy will be reconverted to the ω frequency and will appear as a trailing-edge spike of output at ω, following the signal turn-off.

Fig. 7 illustrates the general appearance of these leading- and trailing-edge leakage spikes.

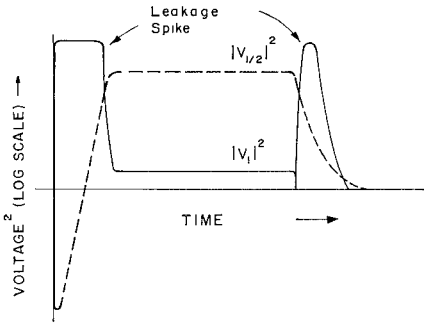

Fig. 7—Output power vs time for a rectangular input pulse, showing leading- and trailing-edge leakage spikes and the buildup of the subharmonic oscillations (dashed line).

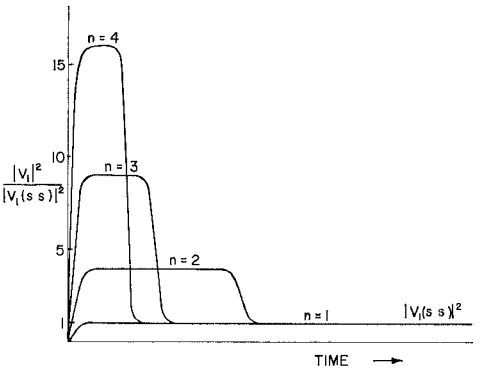

Fig. 8—Leading-edge leakage spikes in a varactor diode limiter for various inputs above the threshold level, as obtained from numerical computations. Parameters are: $f=3$ kMc; $Q_T=5$; $Q_{1/2}=50$; $C_1=C_{1/2}=2.8$ pf; $D=0.28$ pf/v. The input levels $n=2$, 3 and 4 correspond, respectively, to inputs which are 6, 9.6 and 12 db above the threshold level.

Calculations

As part of the work (2) and (3) were solved by numerical forward integration using a large digital computer and small forward steps in time following the application of a signal pulse. Examination of (3) will show that no subharmonic voltage $V_{1/2}$ will ever be developed unless some initial excitation is present to be parametrically pumped up. The initial excitation in the physical case is, of course, thermal noise fluctuations, and these were represented in the calculations by putting in an initial amplitude of $V_{1/2}$ corresponding to the rms thermal noise voltage of the conductance in the $\omega/2$ tank. (The noise voltage was actually reduced by 3 db to account for the fact that only half of the noise energy would be in the proper phase to be pumped up, the other half being so phased as to be parametrically pumped down to zero.) Fig. 8 shows the observed behavior of the output voltage and the subharmonic voltage predicted by the numerical calculations for several different excitations above the threshold level. The input signal is assumed to be an ideal step function, and the numerical parameters are typical values for a varactor diode limiter. It is apparent that the leakage spikes are extremely brief, on the order of nanoseconds, since the pump-up of the subharmonic oscillations is very rapid. The leakage energies are correspondingly small, on the order of 10^{-9} joules.

The exponential nature of the subharmonic buildup has been pointed out in previous studies of parametron oscillators and ferrite limiters [5], [13], [14]. It can be readily derived by rewriting (3) in the form

$$\frac{d}{dt}|V_{1/2}| = -\frac{\omega}{4Q_{1/2}}|V_{1/2}| - j\frac{\omega}{2}\frac{|V_1|}{V_d}\exp j(\theta_1 - 2\theta_{1/2})|V_{1/2}|, \quad (34)$$

where θ_1 is the phase angle of V_1 and $\theta_{1/2}$ the phase angle of $V_{1/2}$. If $V_{1/2}$ is divided into two quadrature components with phase angles $\theta_{1/2}=\theta_1/2+135°$ and $\theta_{1/2}=\theta_1/2+45°$, the former will be parametrically amplified and the latter parametrically deamplified. If V_1 is assumed to very rapidly reach the nonlimited value given by $|V_1|=nV_{th}=nV_d/2Q_{1/2}$, then the subharmonic oscillation voltage grows as

$$|V_{1/2}| = |V_{1/2}(0)| \exp[(n-1)\omega t/4Q_{1/2}]. \quad (35)$$

The length of the initial leakage spikes is essentially the buildup time required for $V_{1/2}$ to grow from its initial noise value to the steady-state value given by (18). The initial noise value is given by $V_{1/2}^2=2kTB_{1/2}/G_{1/2}$ (halved because only growing components are included), and a reasonable value for $B_{1/2}$ would seem to be the bandwidth of the $\omega/2$ tank, $B_{1/2}=\omega 2Q_{1/2}$. With these assumptions, the buildup time or leakage spike length is given by

$$\tau = \frac{2Q_{1/2}}{(n-1)\omega}\ln\left[\frac{(n-1)C_{1/2}V_dV_d'}{4kTQ_TQ_{1/2}}\right]. \quad (36)$$

The argument of the logarithm is the ratio of the steady-state subharmonic oscillation power level to the thermal noise power level, which is a very large ratio, on the order of 120 db for typical values. Therefore, the logarithm is insensitive to the exact value of the thermal noise level, and changes of ± 20 db in the assumed thermal noise level have only a small effect on τ. Fig. 9 shows on a logarithmic scale a comparison between the exponential build-up of $V_{1/2}$ as given by (35) and the results for the same case as obtained from the numerical computer solutions. (The small difference at the initial level is due to different detailed assumptions about the noise level from which the oscillation grows.)

The $Q_{1/2}$ of the $\omega/2$ tank is apparently an important parameter in determining the length of the leakage spikes. This value is fairly low ($\sim$100) in the varactor diode case, which, coupled with a fairly strong degree of nonlinearity, leads to a short leakage spike. Ferrite and garnet limiters operating on this same principle are observed to have substantially longer leakage spikes. This is, in part, due to the relatively higher Q of the spin waves which play the role of the $\omega/2$ tank in the ferrite case.

In work by one of the authors [2], considerable attention is given to the details of the crossover region when

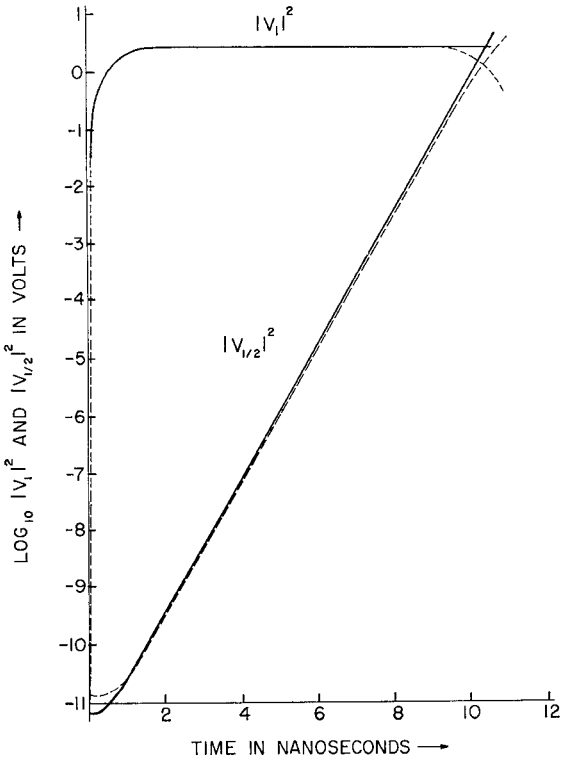

Fig. 9—Exponential buildup of the subharmonic oscillations during the leading-edge spike. Dashed line = computer solution; solid line = analytical solution. Numerical parameters are the same as in Fig. 8, with $n = 16$ (24 db above threshold).

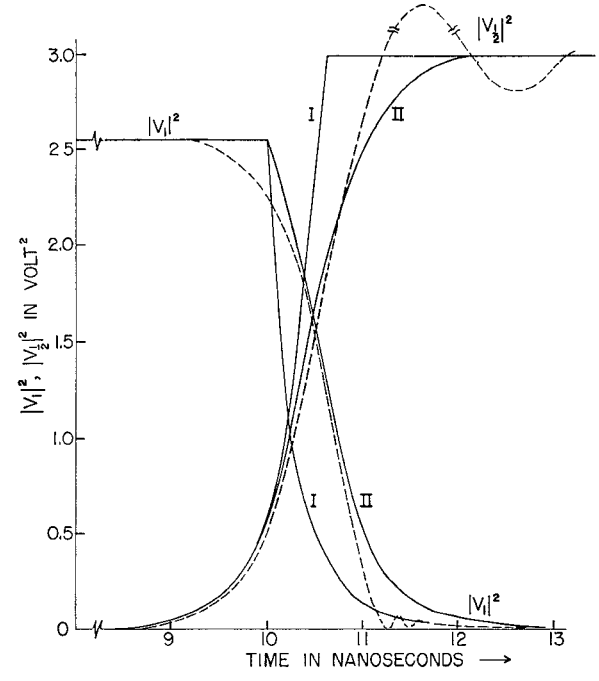

Fig. 10—Details of the limiter behavior in the crossover region from the leading-edge spike to the steady-state limiting condition. Dashed line = computer solution; solid lines I and II = two successive analytic approximations. Numerical parameters are the same as in Fig. 9.

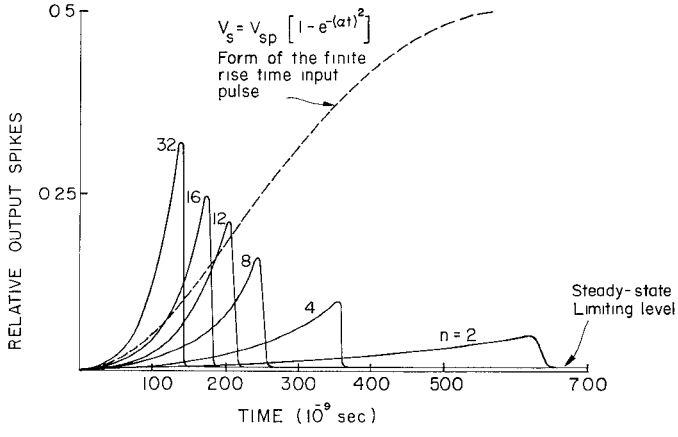

Fig. 11—Leading-edge leakage spikes in a varactor diode limiter for a finite rise time input signal. Numerical parameters are the same as in Fig. 8 with the exception of the input signal. Note difference in shape and length of leakage spikes from Fig. 8.

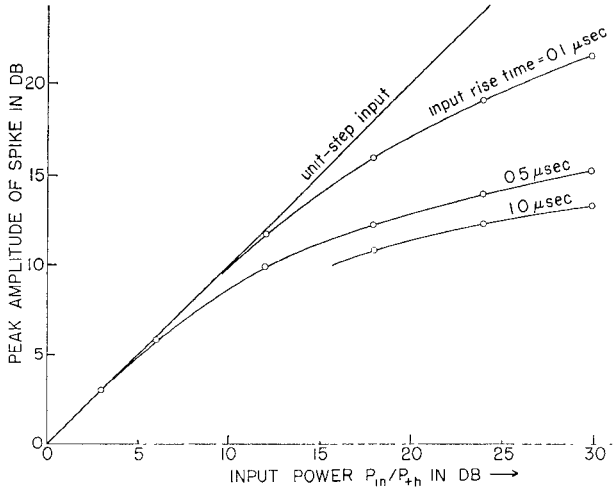

Fig. 12—Curves illustrating the "saturation" behavior of leakage spikes like those in Fig. 11 for input signals of different rise times. Obtained from computer solutions; numerical parameters same as previously.

$V_{1/2}$ nears its steady-state value and the limiting action begins. Iterated piecewise analytic expressions are developed to study the behavior in this region. Fig. 10 shows some of the details of this region, with the numerical computer solution indicated by a dashed line, two successive analytical approximations indicated by solid curves I and II. In general, it can be said that there is a smooth and rapid transition from the initial buildup region to the steady-state limiting region, with only small overshoots and other extraneous effects.

The shortness of the initial leakage spikes in the varactor diode limiter, as compared to typical rise times for pulsed sources, led to consideration of the buildup and leakage spikes in the parametric limiter with finite-rise-time pulses applied. Fig. 11 illustrates the leakage spikes obtained from the computer solution for increasing input power levels when the input signal has a finite rise time. It is observed that the leakage spikes

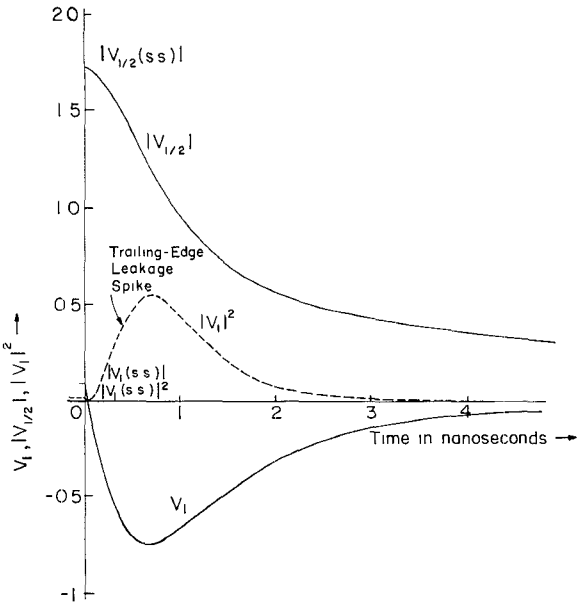

Fig. 13—Trailing-edge leakage spike as obtained from the numerical solutions. Numerical parameters same as in previous figures, with $n=16$.

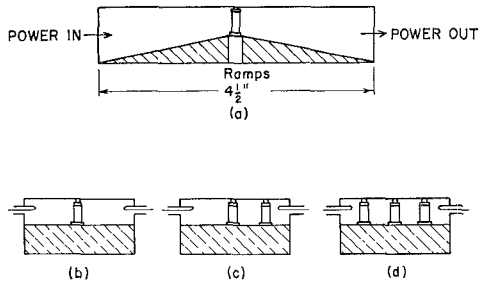

Fig. 14—*S*-band waveguide version of the parametric limiter. (a) Side view; (b), (c), (d) end views of models having one, two and three diodes. The loops are for monitoring the subharmonic resonance.

are shorter at higher input levels, as in the step-function input case, but the spike heights do not continue to rise as the input power is increased. For higher input powers, the subharmonic oscillations have built up to the limiting level before the input pulse is fully built up to its maximum level. The leakage spike height appears to "saturate" at higher input levels. Fig. 12 verifies this by showing the initial leakage-spike height as a function of input power above threshold for several different rise times and a typical set of varactor diode limiter parameters.

The Trailing-Edge Spike

The numerical computation method was also used to obtain the trailing-edge spike characteristics by using the steady-state limited values as initial conditions and solving (2) and (3) with the driving current I_1 set to zero. Fig. 13 shows the trailing-edge leakage spike for a typical case. Note that the subharmonic voltage is much larger than the limited signal voltage in the steady-state situation. Note also that the signal voltage amplitude V_1 drops to zero and then changes sign. This corresponds to V_1 changing from the driving to the driven quantity in the parametric circuit.

It should be noted that there can be an entirely independent source of leakage spikes in practical situations. If the frequency of the pulsed signal source changes during the rise and fall of the signal pulse, as may well be the case with some pulsed signal sources, this can also cause a significant leakage spike on the trailing edge of the limited pulse.

Experimental Results

Three versions of parametric limiters using varactor diodes as nonlinear devices were built and tested during this work, and a fourth version using a YIG sphere as its nonlinear element was borrowed from the Watkins-Johnson Co. and tested. Each version served a different purpose in verifying the theoretical predictions given in the previous sections. These four versions [2] were:

1) An *S*-band waveguide version used for some initial experiments, characterized by no resonant tank at the ω frequency and employing several Microwave Associates, Inc., MA460 varactor diodes in parallel shunted across the waveguide.

2) An *S*-band YIG sphere version used for observing the leakage spikes, since these are too short to be readily seen in the *S*-band varactor diode-type limiter.

3) A VHF (126 Mc) lumped-circuit version again employing MA460 varactor diodes used to observe the leakage spikes by virtue of its lower signal frequency.

4) An *S*-band strip-line version employing a Microwave Associates Inc., MA4253 pill-type varactor diode with the twin virtues of low-series inductance and high-cutoff frequency, used for detailed comparisons with the steady-state theory given above.

S-Band Rectangular Waveguide Version

A parametric limiter with one or more MA 460 varactor diodes installed inside an *S*-band rectangular waveguide was first designed and built as shown in Fig. 14. The detection loops were for monitoring the $\omega/2$ oscillation. The important features of this design were:

a) There was no ω resonant tank. One, two, or three diodes were simply placed side by side across the waveguide, whose height was reduced by ramps before and after the diodes. The waveguide was propagating at the signal and all higher frequencies, but was well below cutoff at the subharmonic frequency.

b) A novel method was employed for obtaining the $\omega/2$ resonance. The imaginary characteristic impedance of the rectangular waveguide below cutoff, which for the TE_{10} mode is inductive in nature, was resonated with the diode capacitance to create the subharmonic resonance at the $\omega/2$ frequency. This type of resonance is sometimes called a "ghost mode" [15]. The subharmonic resonance was tuned by varying the reverse bias, thus changing the dc capacitance of the diode.

Measurements of output limiting were conducted separately for the three diode arrangements shown in Fig. 14. They all yielded similar sharp limiting as predicted for a parametric limiter. However, the dynamic range of limiting increased considerably with more diodes.

	1 diode	2 diodes	3 diodes
Signal frequency	3040 Mc/sec	2878 Mc/sec	2738 Mc/sec
Dynamic range of limiting	3 db	7.5 db	16 db
Bias	−1.5 v	−1.5 v	−1.5 v
Threshold level	~10 mw	~10 mw	~10 mw

Approximately a ten per cent bandwidth was obtainable in the limiting of these three cases. Phase-distortion measurements showed that the phase distortion of the 3-diode limiter was less than $\pm 3°$, which is the accuracy of the measurement, over the entire 16-db range of limiting. Insertion loss of the 3-diode limiter below threshold was approximately 10 db. This configuration represents a particularly simple form for such a limiter and may merit further development.

S-Band Yttrium Iron Garnet Sphere Version

Leakage spikes were too short to be readily seen in the previous *S*-band varactor diode limiter. The theoretical duration time of the leading-edge leakage spike is found to be on the order of 10^{-9} second when reasonable values for the parameters are substituted into (36). To make τ long enough to be easily observable, two alternatives were tried, one by using a YIG sphere limiter because of its higher $Q_{1/2}$, the other by using a VHF version (126 Mc) to lower the ω. The results of the YIG sphere version are shown in this section, and those of the VHF version are shown in the next section.

The leading-edge leakage spikes are shown in Fig. 15. The duration times of the leakage spikes become shorter as the input power increases. The peak amplitudes of the leakage spikes increase first and then saturate. The

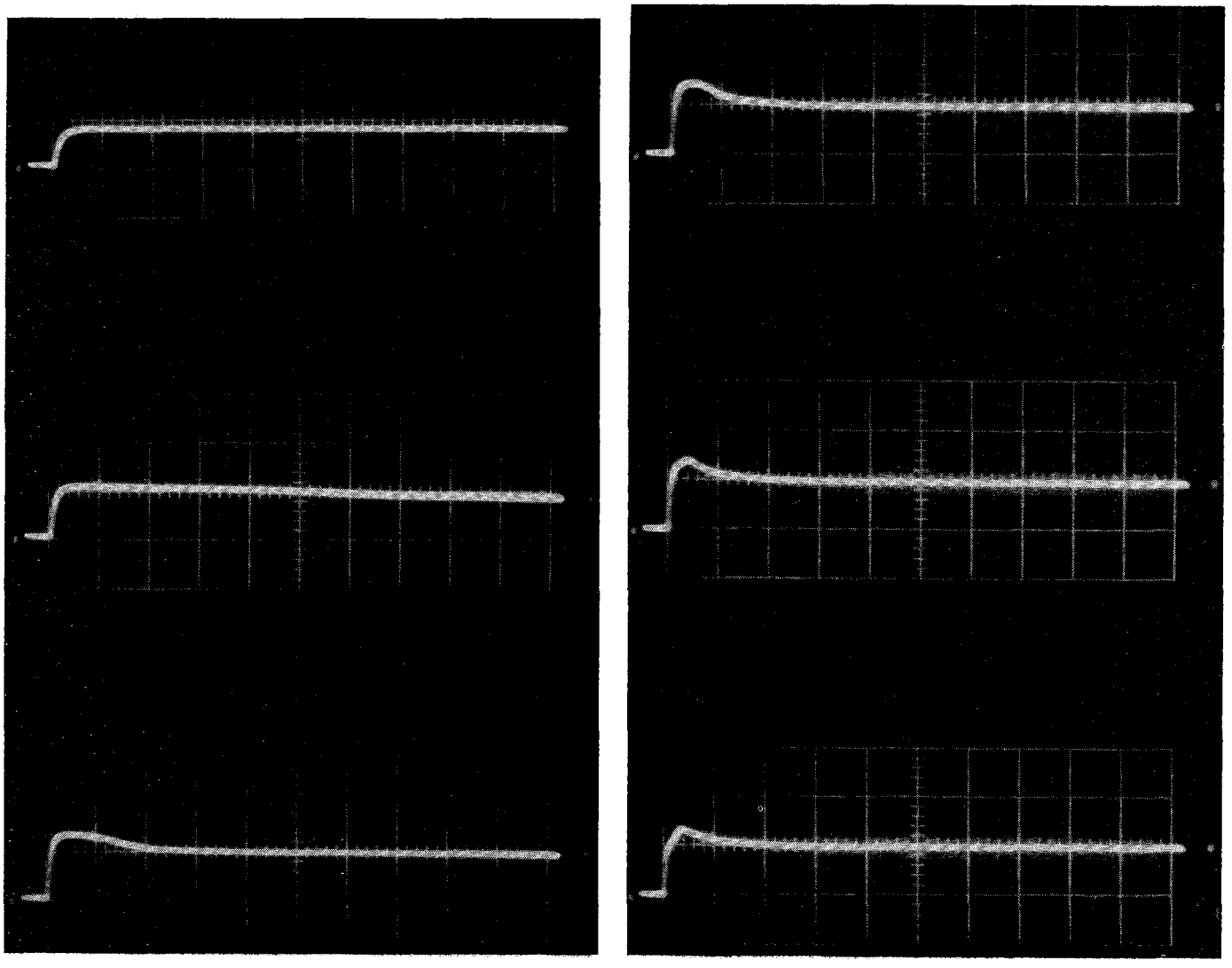

(a) (b)

Fig. 15—Leakage spikes observed in a garnet sphere form of parametric limiter. The behavior of the leakage spikes is in qualitative agreement with the theory.

qualitative behavior of the leading-edge leakage spikes at first agrees in general with the theoretical predictions, although detailed quantitative comparisons are not possible because the basic parameters for the garnet sphere limiter are not known. The insertion loss of this version was measured to be 5 db, and the dynamic range was over 20 db.

VHF Lumped Circuit Version

From (36) one realizes that a lower signal frequency ω will also make the duration time of the leading-edge leakage spike longer. A lower-frequency (126 Mc) limiter was therefore built by shunting three MA460 varactor diodes with a lumped circuit coil to form a $\omega/2$ tank and then placing band-pass filters at $f=126$ Mc on each side of this circuit. The $\omega/2$ tank was tuned to 126/2 Mc with a 1-v reverse bias applied on the varactor diodes. The leading edges of the output waveforms are shown in Fig. 16, which were taken on a wideband oscilloscope without using a crystal detector. As in Fig. 15, the leading-edge leakage spikes saturate quite rapidly.

The insertion loss of this version is measured to be 3 db; its dynamic range is 10 db. The threshold level of this limiter was measured to be 2.4 db above a milliwatt, and a more than 5 per cent bandwidth was observed.

S-Band Stripline Version

The recently available pill-type varactor diode has the twin advantages of low series inductance and high-cutoff frequency. Its tiny size of $\frac{1}{8}$ in $\times\frac{1}{8}$ in fits a stripline configuration better than other microwave configurations, and hence a stripline limiter was designed. The pill varactor used in this work had a zero-bias

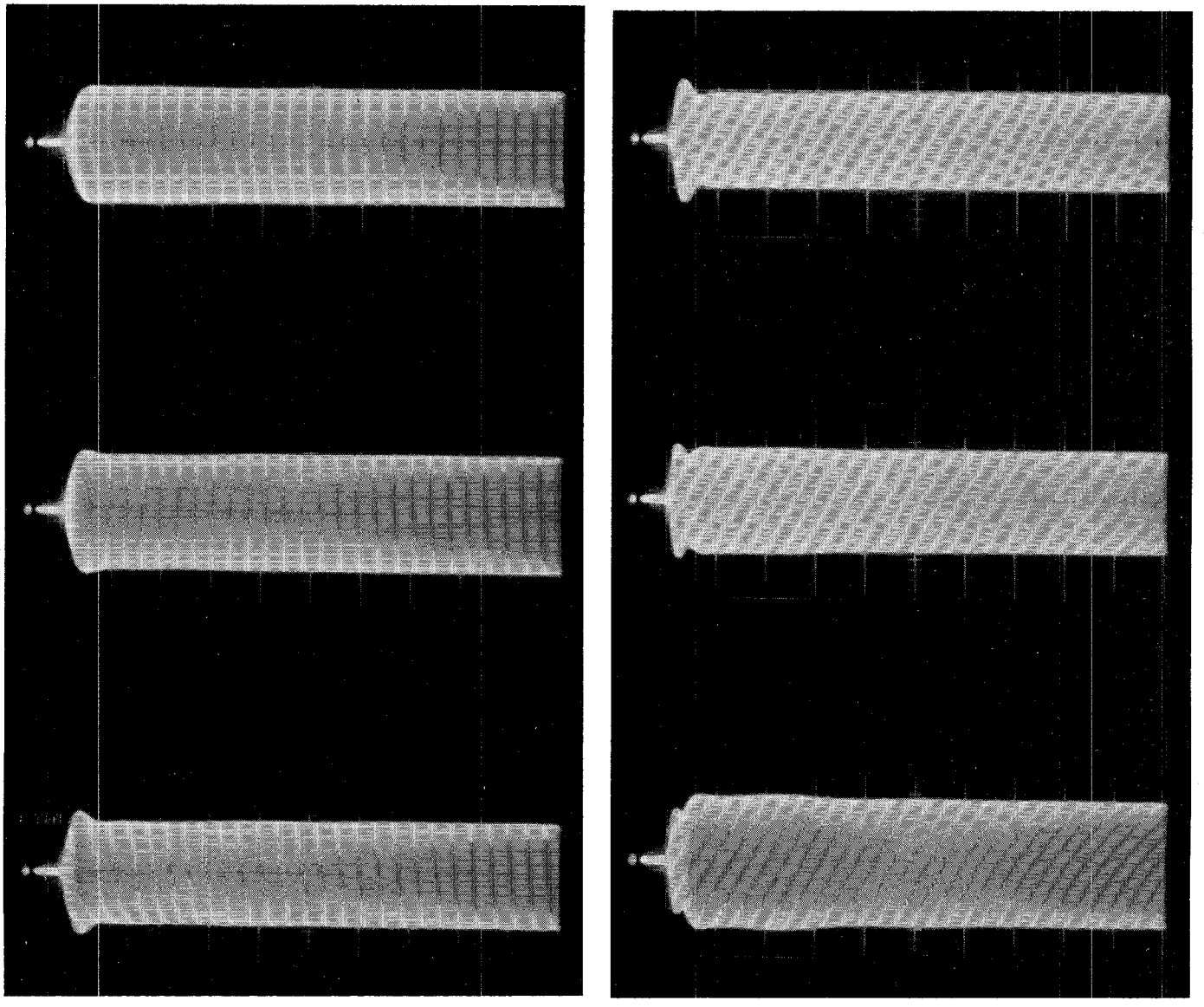

(a) (b)

Fig. 16—Leakage spikes observed in a varactor diode limiter operating at 126 Mc. Again, there is qualitative agreement with the theory, at least at the lower power levels.

capacitance of 0.78 pf and a cutoff frequency of 126 kMc.

The pill varactor was mounted between the center conductor and one of the ground planes of the strip-line. Two movable shorts, one on each end of the strip-line, together with the change in varactor dc capacitance with change in bias voltage, served to adjust the resonant frequencies of this device. Fig. 17(a) shows a side view of the limiter, and Fig. 17(b) shows the electric field distributions for the ω and $\omega/2$ resonant modes employed. Signal power was coupled into and out of the ω tank by two loops located at a position where the magnetic field of the ω mode was maximum while that of the $\omega/2$ mode was minimum. A pair of monitoring loops was also placed at a position where the magnetic field of the ω mode was zero in order to monitor the subharmonic oscillations and perform tuning adjustments at $\omega/2$. Diode dc isolation and RF bypass were obtained by placing below the pill varactor a capacitor formed by 1" diameter copper disk with a 5-mil thick teflon dielectric. The lower-ground plane was countersunk to a depth such that the top of the copper disk was flush with the remaining surface of the lower-ground plane. Fig. 18 shows photographs of this limiter assembled and disassembled.

With this limiter, essentially flat limiting over a range of 20 db above a threshold level of ~1 mw was observed, as shown in Fig. 19. Insertion loss below threshold was ~2.5 db. The phase distortion was measured both below and above the threshold level with the results shown in Fig. 20. Over the entire input power range, the phase distortion is within $\pm 5°$, the accuracy of measurement being approximately $\pm 3°$.

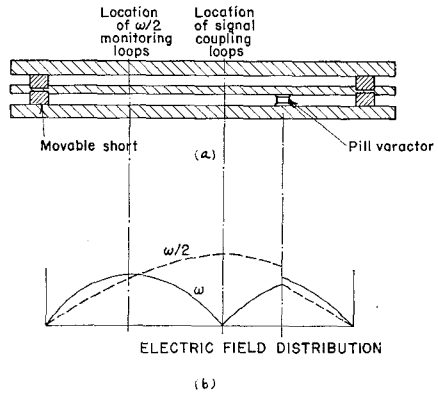

Fig. 17—Side view of the strip-line varactor diode limiter, and mode patterns of the resonant modes at ω and $\omega/2$.

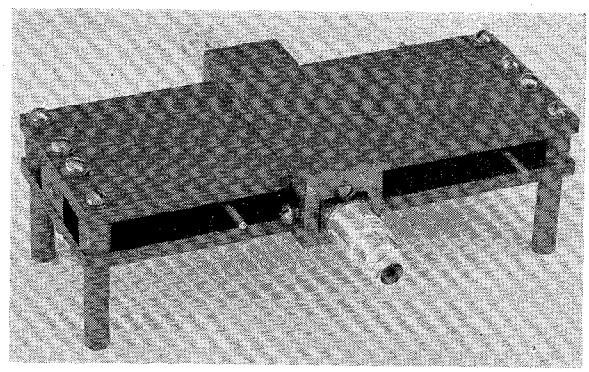

(a)

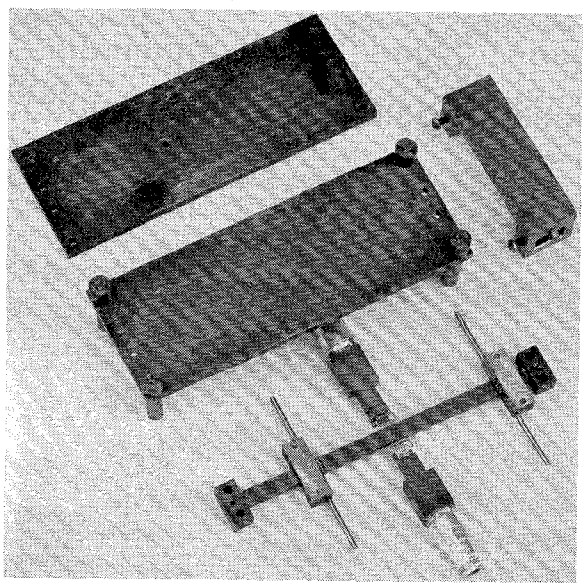

(b)

Fig. 18—Assembled and exploded view of the strip line limiter ($\omega/2$ coupling loops not shown).

Comparison with Theory

The strip-line limiter operated at a reverse bias of 1.0 v had the following characteristics, as determined from the known diode characteristics plus careful measurements of the below-threshold characteristics of the resonant modes at ω and $\omega/2$:

$\omega_0 = 2382$ Mc

$Q_T = 41$

$Q_{1/2} = 117$

Input VSWR = 1.2

$G_L = G_g = 20 \times 10^{-3}$ mhos

$G_T = G_1 + 2G_g \approx 44 \times 10^{-3}$ mhos

$V_d = V_d' \approx 40$ v

$V_{br} = 5.5$ v

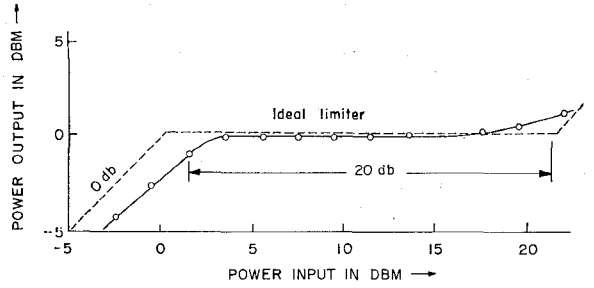

Fig. 19—Limiting characteristic of the strip-line varactor diode limiter showing a 2-mw threshold level and a 20-db dynamic range.

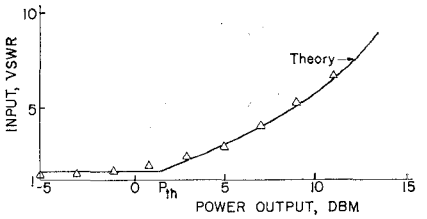

Fig. 21—Input VSWR to the limiter as a function of input power level, compared to the theoretical expression of (16).

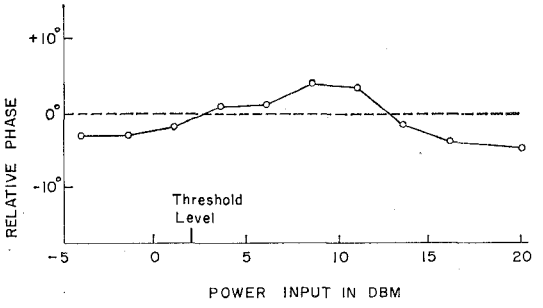

Fig. 20—Relative phase of the limiter output compared to limiter input as a function of input power level, showing the phase-distortionless nature of the parametric limiting.

One can substitute these parameters into the various theoretical expressions given above and compare them with the experimental results. The following comparisons will show the excellent agreement obtained:

a) *Threshold level:* Use of the above numbers in (8) and (9) gives a predicted threshold level of 1.25 mw. The measured value is approximately 2 mw.

b) *Phase distortion:* As shown in Fig. 20, the phase distortion is very small, nearly within the error of measurement, in agreement with theoretical predictions.

c) *Input VSWR above threshold:* Eq. (16) relates the input VSWR above threshold to the value below threshold and the value of n. Fig. 21 shows the comparison between this equation and the experimental results obtained on the stripline limiter. A similar input VSWR curve given by Wolf and Pippin [3] was also compared with (16), and good agreement was again obtained.

d) *Dynamic range:* From (19) and (20), the predicted dynamic range is $n_{max}=12.4$ or a dynamic range of 22 db. The measured value, as determined by the point at which the power output curve of Fig. 19 begins to rise, is approximately 20 db.

e) *Bandwidth:* The power output vs frequency characteristics of the limiter at different input power levels were studied with the aid of a swept-frequency RF source, leading to the oscilloscope traces of detected output vs frequency shown in Fig. 22. Since the output of the swept-frequency source was not leveled and various mismatches are present in the system, detailed com-

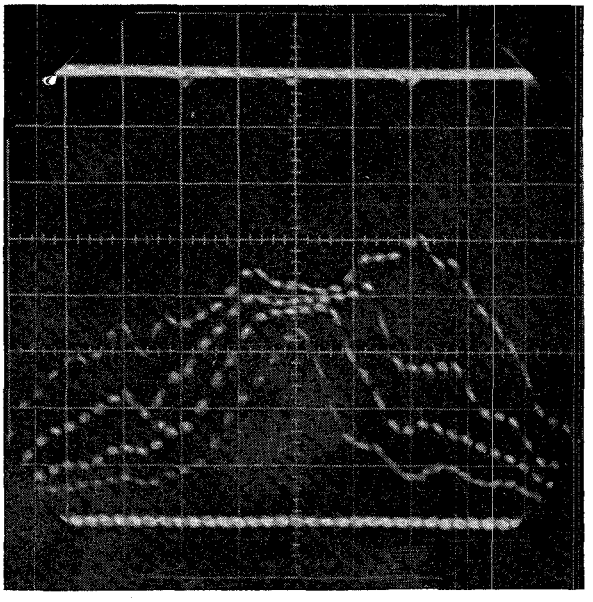

(a)

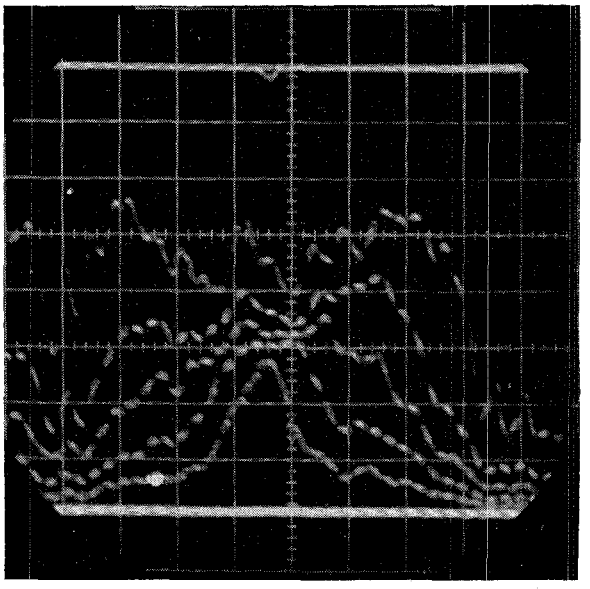

(b)

Fig. 22—Strip-line limiter power output vs frequency for various input powers, using a nonleveled swept signal generator, for comparison with Fig. 6.

parison of these results with the theoretical curves of Fig. 6 is not possible, but it can be seen that the general nature of the curves agrees well with the theoretical predictions. There appears to be a slight drift of the center quency of the limiter with increasing power level, which is attributed to a shift in the dc capacitance due to second-order effects, since the amount of this shift was dependent on the stiffness of the dc bias supply.

In general, it seems fair to conclude that excellent agreement is obtained between these measurements and the theoretical formulas developed earlier in this paper.

Conclusions

The passive parametric limiter offers several features, including, a) a sharp limiting threshold; b) flat power output for a substantial dynamic range above the threshold; c) little or no phase distortion; d) conveniently low-threshold power levels; and e) simple construction, with no auxiliary pumps, power supplies, or equipment (other than a simple dc bias supply) being required. Such limiters can be built at essentially any frequency from the audio to the microwave range, and may find employment either in protective applications or in signal-processing applications, particularly those where the phase-distortionless feature is essential. The present work has presented design equations and data for parametric limiters employing varactor diodes, together with experimental results at VHF and microwave frequencies which indicate the performance characteristics of such limiters. The excellent agreement between theory and experiment gives substantial confidence in the accuracy of the design equations.

References

[1] A. E. Siegman, "Phase-distortionless limiting by a parametric method," Proc. IRE, vol. 47, pp. 447–448; March, 1959.
[2] I. T. Ho, "Passive Phase-Distortionless Parametric Limiter," Stanford Electronics Labs., Stanford, Calif., Tech. Rept. 157-2; April, 1961; also Ph.D. dissertation, Dept. of Elec. Engrg., Stanford Univ., Stanford, Calif.; April, 1961.
[3] A. A. Wolf and J. E. Pippin, "A passive parametric limiter," 1960 Internatl. Solid State Circuits Conf. Digest of Tech. Papers, Philadelphia, Pa., pp. 90–91; February, 1960.
[4] R. W. Degrasse, "Low-loss gyromagnetic coupling through single crystal garnets," *J. Appl. Phys.*, vol. 30, pp. 155S–156S; April, 1959.
[5] G. S. Uebele, "Characteristics of ferrite microwave limiters," IRE Trans. on Microwave Theory and Techniques, vol. MTT-7, pp. 18–23; January, 1959.
[6] A. D. Sutherland and D. E. Countiss, "Parametric phase-distortionless *L*-band limiter," Proc. IRE, vol. 48, p. 938; May, 1960.
[7] F. A. Olson, *et al.*, "Parametric devices tested for phase-distortionless limiting," Proc. IRE, vol. 47, pp. 587–588; April, 1959.
[8] W. Shockley, "Theory of p-n junctions in semiconductors and p-n junction transistors," *Bell Sys. Tech J.*, vol. 28, pp. 436–489; July, 1949.
[9] A. Uhlir, Jr., "Varactors," Microwave Associates, Inc., Burlington, Mass., Brochure 59V; February, 1959.
[10] H. Heffner and G. Wade, "Gain, bandwidth, and noise characteristics of the variable-parameter amplifier." *J. Appl. Phys.*, vol. 29, pp. 1321–1331; September, 1958.
[11] J. M. Manley and H. E. Rowe, "Some general properties of nonlinear elements—Part I: General energy relation," Proc. IRE, vol. 44, pp. 904–913; July, 1956.
[12] J. Von Neumann, "Nonlinear capacitance or inductance switching, amplifier, and memory organs," U. S. Patent No. 2,815,488; December 3, 1957.
[13] E. Goto, "The parametron, a digital computing element which utilized parametric oscillation," Proc. IRE, vol. 47, pp. 1304–1316; August, 1959.
[14] "X-band ferrite limiter," Hughes Aircraft Co., Component Div., Culver City, Calif. Interim Engrg. Repts. I–IV: September, 1959–June, 1960.
[15] E. T. Jaynes, "Ghost modes in imperfect waveguides," Proc. IRE, vol. 46, pp. 416–418; February, 1958.
[16] F. A. Olson and G. Wade, "A cavity-type parametric circuit as a phase-distortionless limiter," IRE Trans. on Microwave Theory and Techniques, vol. MTT-9, pp. 153–157; March, 1961.

Solid-State *X*-Band Power Limiter*

W. F. KRUPKE†, T. S. HARTWICK‡, and M. T. WEISS‡, senior member, IRE

Summary—**An *X*-band solid-state power limiter has been designed and built to protect receiver crystals from high-power microwave pulses in the kilowatt region. This passive and reliable crystal protection has been achieved by utilizing the nonlinear properties of both ferrites and semiconductor diodes. An understanding of the ferrite nonlinear mechanism, which gives rise to the characteristically large leakage spike, has been achieved and quantitatively described. This formulation resulted in an essentially optimized high-power ferrite limiter, whose mode of operation is qualitatively understood. Use of this ferrite limiter for crystal protection requires a fast response, lower threshold secondary-limiting unit, which was developed by using semiconductor diodes for power limiting in a reactive mode of operation. The ferrite and diode limiters were combined in a single device with an over-all insertion loss of 2.0 db and a 200-Mc operating "bandwidth."**

* Received by the PGMTT, May 15, 1961; revised manuscript received, June 29, 1961. This paper is based on work performed at Hughes Aircraft Co., Culver City, Calif., and supported by the Bureau of Ships, Dept. of the Navy, under Contract NObsr-77605.

† Aeronatucial Div., Minneapolis-Honeywell Co., Los Angeles, Calif.

‡ Electronics Lab., Aerospace Corp., El Segundo, Calif.